

# Surface structure and phase transition of K adsorption on Au(111): By *ab initio* atomistic thermodynamics

Li-Yong Gan,<sup>1,2</sup> Ren-Yu Tian,<sup>1</sup> Xiao-Bao Yang,<sup>1</sup> and Yu-Jun Zhao<sup>1,2,a)</sup>

<sup>1</sup>Department of Physics, South China University of Technology, Guangzhou 510640, People's Republic of China

<sup>2</sup>State Key Laboratory of Luminescent Materials and Devices, South China University of Technology, Guangzhou 510640, People's Republic of China

(Received 29 October 2011; accepted 23 December 2011; published online 25 January 2012)

We studied the interactions between atomic potassium (K) and Au(111) at a range of coverage (i.e.,  $\Theta_K = 0.11$ –0.5 monolayer (ML)) by *ab initio* atomic thermodynamics. For K on-surface adsorption, we found that K energetically favors the three-fold hollow sites (fcc or hcp), while the most significant surface rumpling was obtained at the atop sites. The incorporation of gold atoms in the adsorbate layer gradually becomes energetically favorable with increasing K coverage. We proposed a possible model with a stoichiometry of  $K_2Au$  for the  $(2 \times 2)$ –0.5 ML phase observed in lower energy electron diffraction (LEED): one K at atop site and the other K as well as one Au adatom at the second-nearest fcc/hcp and hcp/fcc, respectively. Clear theoretical evidences were given for the *ionic* interaction of K on Au surface. Additionally, phase transitions were predicted based on chemical potential equilibrium of K, largely in line with the earlier reported LEED observations: the clean surface  $\rightarrow (\sqrt{3} \times \sqrt{3})R30^\circ \rightarrow (2 \times 2)$ , and  $(2 \times 2) \rightarrow (\sqrt{3} \times \sqrt{3})R30^\circ$  reversely at an elevated temperature. © 2012 American Institute of Physics. [doi:10.1063/1.3678842]

## I. INTRODUCTION

Over the last several decades, the adsorption of alkali metals (AMs) on transition metal (TM) surfaces has always been one of the most attractive issues in the surface science.<sup>1–5</sup> Technologically, AMs can be used to increase electron emission rates and also as efficient promoters in electrochemistry and heterogeneous catalysis.<sup>6–8</sup> Scientifically, AM adsorption is one of the simplest processes but exhibits extremely rich physical and structural behaviors. Stimulated by the two reasons, a renewed interest of AM adsorption has emerged recently. For example, Pratt *et al.*,<sup>9</sup> using a serial of experimental tools, examined the coverage and temperature dependent behavior of the potassium adsorption on Pd(110) surface. Theoretically, many simulations<sup>10–14</sup> have been carried out to either investigate the interactions between AM and substrates or ascertain the composite surface structures. It has been shown that the AM adatoms may be either adsorbed at the on-surface (i.e., atop, bridge, fcc, and hcp) and substitutional sites to form an adlayer,<sup>12,15–19</sup> or be incorporated in the adsorbate layer to yield an intermixed surface alloys.<sup>10,20,21</sup> Specifically, the system of AM/Au(111) is therefore such an interesting system due to the “gold rush” since 1987 by Haruta.<sup>22</sup>

Potassium (K) adsorption on Au(111) exhibits extraordinary rich phase behaviors, which are greatly dependent on the coverage ( $\Theta$ ) and temperature ( $T$ ). This may partly be ascribed to the presence of the  $(22 \times \sqrt{3})$  reconstructions<sup>23</sup> of the clean surface. Barth *et al.*<sup>24</sup> carried out low energy electron diffraction (LEED) and scanning tunnel microscope mea-

surements to explore K adsorption at various  $\Theta_K$  and  $T$ , and a series of structural transformations were observed. For  $\Theta_K \leq 0.33$  monolayer (ML), the periodicity of the Au(111) Clevron structure  $(22 \times \sqrt{3})$  decreases as the coverage of K increases. At  $\Theta_K = 0.33$  ML, the K adatoms form a hexagonal  $(\sqrt{3} \times \sqrt{3})R30^\circ$  overlayer, in agreement with results of other systems, e.g., K/Pt(111).<sup>25</sup> For  $\Theta_K = \sim 0.5$  ML, the Au(111) reconstruction is completely lifted, and meanwhile a  $(2 \times 2)$  LEED pattern is observed. This phase was assigned to an Au–K intermixed layer. For  $\Theta_K > 0.60$  ML, the pattern becomes more and more diffuse and the spots are hardly visible at  $\Theta_K = \sim 0.9$  ML.<sup>21,24</sup> Unfortunately, the detailed surface structures, especially the  $(2 \times 2)$  phase, are still unclear.

The state-of-the-art density functional theory (DFT) calculations have been verified to be such a powerful and effective tool which can provide qualitative and (in many cases) quantitative insights into surface science,<sup>26</sup> including the AM adsorption.<sup>10</sup> In the present work, we carried out periodic DFT calculations to investigate K adsorption on Au(111) at  $\Theta_K \leq 0.5$  ML,<sup>24</sup> aiming at getting an insight into the behaviors and interactions of K on Au(111). This is very important for the understanding of both structural and chemical properties of the gold surface. From our calculations, we found the possible  $(2 \times 2)$  intermixed Au–K phase as following: two K atoms occupy a hollow site (either fcc or hcp) and an atop site each, while the incorporated Au adatom is located at the other corresponding hollow site (either hcp or fcc in turn). Further calculations of the surface free energies of K/Au, considering the temperature and pressure ( $T, p$ ) dependence through the chemical potential of K, provide an unambiguous picture for the structural transformation, in excellent agreement with the observed LEED patterns. In addition to the structural determi-

<sup>a)</sup> Author to whom correspondence should be addressed. Electronic mail: zhaoyj@scut.edu.cn. Tel.: +86-20-87110426. Fax: +86-20-87112837.

nation, the corresponding electronic structures were also discussed to get a better understanding of the K/Au(111) system.

## II. MODEL AND METHODOLOGY

This work was conducted by the Vienna *ab initio* simulation package<sup>27–30</sup> with the frozen-core projector-augmented-wave (PAW) method.<sup>31,32</sup> The Perdew Wang (PW91) generalized gradient approximation functional<sup>33,34</sup> was employed for the exchange-correlation energy. The PAW pseudopotential of K<sub>p</sub>v, in which the semi-core *s* and *p* states were both treated as the valence electrons, was used. The Fermi level was smeared by the first-order Methfessel-Paxton<sup>35</sup> approach with a width of 0.2 eV. The adsorption was modeled with a 5-layer slab containing a vacuum thickness of 20 Å. Adatoms (K or Au or both) were placed on one side of the slab. The outermost three layers including all the adatoms were fully relaxed with the residual forces of each relaxed ion less than 0.02 eV/Å, while the two bottommost layers were fixed at their bulk structure with the previous optimized lattice constant, 4.176 Å.<sup>36</sup>

This work was mainly arranged in three parts: the on-surface adsorption ( $\Theta_K = 0.11$ – $0.33$  ML); the intermixed Au–K ( $2 \times 2$ )– $0.25$  ML K phase;<sup>24</sup> the (*T*, *p*) phase diagram of K–Au system with respect to experiment results. In the first part, the simulation has been performed using ( $3 \times 3$ ), ( $2 \times 2$ ), and  $(\sqrt{3} \times \sqrt{3})R30^\circ$  unit cells (shown in Fig. 1) to investigate the coverage dependent K–Au(111) bonding properties (i.e., the amount and nature of charge transfer). The adsorption energy is defined as

$$E_{\text{ads}}(n) = E_{\text{K/Au}} - E_{\text{Au-substrate}} - nE_{\text{K}}, \quad (1)$$

where  $E_{\text{K/Au}}$ ,  $E_{\text{Au-substrate}}$ , and  $E_{\text{K}}$  are the total energies of the K adsorbed Au systems, the corresponding Au(111) substrate, and the free K atom, respectively. In this section,  $E_{\text{Au-substrate}}$  is equal to  $E_{\text{Au(111)}}$ , which represents the *clean* flat Au(111) surfaces, and *n* is the K adatom number, which is equal to 1 for K adsorption on the *clean* flat Au(111) at  $\Theta_K = 0.11$ – $0.33$  ML.

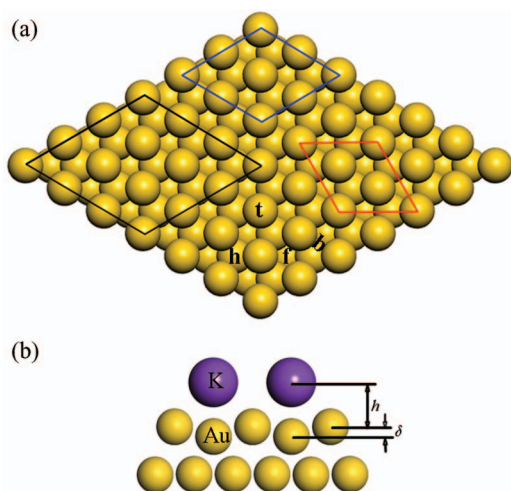


FIG. 1. (a) Top view of the surface unit cell for ( $3 \times 3$ ) (black lines), ( $2 \times 2$ ) (blue lines), and  $(\sqrt{3} \times \sqrt{3})R30^\circ$  (red lines); (b) Definition of the height of K atom from the surface,  $h$  (Å), and the vertical surface rumpling,  $\delta$  (Å). The letters “t,” “b,” “f,” and “h” stand for the top, bridge, fcc, and hcp.

In the second part, Au atom incorporated structures were all calculated in a ( $2 \times 2$ ) unit cell. In order to compare the stability of K adsorption on the Au substrates with various numbers of Au adatoms, the total energy of *n* K adsorption on the Au(111) with *m* gold adatoms ( $m = 1, 2, 3$ ) is calculated as

$$E_{\text{tot}}(n, m) = E_{\text{ads}}(n) + E_{\text{cost}}(m). \quad (2)$$

Of note, the Au substrate here may be with or without extra Au adatoms.  $E_{\text{cost}}(m)$  is the energy cost for creating *m* gold adatoms,

$$E_{\text{cost}}(m) = E_{\text{Au-substrate}} - E_{\text{Au(111)}} - mE_{\text{Au-bulk}}, \quad (3)$$

where  $E_{\text{Au-bulk}}$  represent the total energies of bulk gold (per atom). The approach of Eqs. (1)–(3) has been used to successfully elucidate the phenomenon of Au incorporation upon chlorine adsorption.<sup>37,38</sup> In Ref. 23, it has been demonstrated that the most energetically favorable adsorption site for sulfur on the unreconstructed and reconstructed Au(111) is similar. Additionally, the Cleveron reconstruction would be gradually ruined upon K adsorption and be completely lifted at  $\sim 0.5$  ML of K.<sup>24</sup> Therefore, we did not consider the reconstruction in the present work. Meanwhile, the  $(\sqrt{3} \times \sqrt{3})R30^\circ$  phase was reported to be in agreement with other AM/TM systems in Ref. 24.

In the third part, in order to elucidate the surface structural transition of Au(111) upon K adsorption ( $\Theta_K \leq 0.50$  ML), the surface free energy ( $\gamma$ ) as a function of K chemical potential ( $\mu_K$ ) is calculated as

$$\gamma(T, P) = [G_{\text{K/Au(111)}} - G_{\text{Au(111)}} - N_{\text{Au}}\mu_{\text{Au}} - N_{\text{K}}\mu_{\text{K}}]/A, \quad (4)$$

where  $G_{\text{K/Au(111)}}$  and  $G_{\text{Au(111)}}$  are the Gibbs free energies of the considered K/Au system and the *clean* flat Au(111) reference surface, respectively.  $N_{\text{Au}}$  and  $N_{\text{K}}$  are the numbers of gold atoms (relative to the flat Au surface) and K atoms, respectively. For K adsorption on clean surface and surfaces with one vacancy or *m* Au adatoms,  $N_{\text{Au}}$  are 0,  $-1$ , or *m* in turn.  $\mu_{\text{Au}}$  and  $\mu_{\text{K}}$  are the chemical potentials of Au and K atoms, respectively. Here,  $\mu_{\text{Au}}$  is the free energy for an Au atom in its fcc bulk. *A* is the surface area. It has been shown that the Gibbs free energies of Au surfaces could be approximated by the DFT total energies<sup>39–41</sup> since the contributions from entropy and work done by pressure are relatively small. Therefore, Eq. (7) is updated to

$$\gamma_{\text{DFT}}(T, P) = [E_{\text{K/Au(111)}} - E_{\text{Au(111)}} - N_{\text{Au}}\mu_{\text{Au}} - N_{\text{K}}\mu_{\text{K}}]/A. \quad (5)$$

The *T* and *p* dependence is given by  $\mu_K$ . Since the potassium atoms are evaporated from a source in experiments, the K gas environment is approximated as an ideal gas, in which K chemical potential is given as<sup>42</sup>

$$\mu_{\text{K}}(T, p) = E_{\text{K}} + k_{\text{B}}T \ln p - \frac{5}{2}k_{\text{B}}T \ln(k_{\text{B}}T) - \frac{3}{2}k_{\text{B}}T \ln\left(\frac{2\pi M}{h^2}\right), \quad (6)$$

where  $k_B$  is the Boltzmann constant,  $M$  is the mass of potassium atom, and  $h$  is the Planck constant.

For all the calculations, a cutoff energy of 400 eV was employed for the plane-wave expansion. Brillouin-zone integrations were performed with the  $\Gamma$  centered Monkhorst-Pack<sup>43</sup> grids of  $4 \times 4 \times 1$ ,  $6 \times 6 \times 1$ , and  $7 \times 7 \times 1$   $k$ -points for the  $(3 \times 3)$ ,  $(2 \times 2)$ , and  $(\sqrt{3} \times \sqrt{3})R30^\circ$  unit cells, respectively. The convergence test for the adsorption energies has been carried out with respect to the  $k$ -point sampling, energy cutoff, and the vacuum thickness. It has been shown that higher energy cutoff (500 eV) and denser  $k$ -point sampling for each system vary the adsorption energies less than 10 meV.

### III. RESULTS AND DISCUSSIONS

#### A. K on-surface adsorption

The adsorption energies and structural parameters for K on-surface adsorption at coverage from 0.11 ML to 0.33 ML are listed in Table I. At the three studied coverage, the most energetically preferred sites are the three-fold hollow sites (fcc or hcp) with the adsorption energies ( $E_{\text{ads}}$ ) from  $-2.57$  eV ( $\Theta_K = 0.11$  ML) to  $-1.98$  eV ( $\Theta_K = 0.33$  ML). The potential energy surface for K on Au(111) is rather smooth since the adsorption energies at the least energetically favorable sites, namely, atop, are only higher by 100 meV, correspondingly. Increasing K coverage weakens the K–Au interactions due to the strengthened repulsion between K adatoms at a higher coverage. To get a more detailed understanding of the interactions between the K adsorbates and Au(111), we then decomposed the adsorption energy into three parts,<sup>13,15</sup>

TABLE I. Adsorption energies,  $E_{\text{ads}}$ , and structural parameters for K on Au(111) at the coverage of 0.11, 0.25, and 0.33 ML. Heights of K from the surface,  $h$ , K–Au bond lengths,  $d_{\text{K–Au}}$ , effective radii of K,  $R_{\text{eff}}$ , and surface vertical rumpling,  $\delta$ , respectively. The adsorption sites are defined in Figs. 1 and 5.

Site	$E_{\text{ads}}$ (eV)	$h$ (Å)	$d_{\text{K–Au}}$ (Å)	$R_{\text{eff}}$ (Å)	$\delta$ (Å)	Charge <sup>a</sup> (e)
$\Theta = 0.11$ ML						
t	-2.48	3.815	3.03	1.554	0.214	+0.84
b	-2.56	2.690	3.22	1.744	0.090	+0.84
f	-2.57	2.711	3.31	1.834	0.044	+0.84
h	-2.57	2.716	3.31	1.834	0.046	+0.84
s	-2.31	1.717	...	...	...	+0.84
$\Theta = 0.25$ ML						
t	-2.12	2.585	2.96	1.484	0.370	+0.73
b	-2.18	2.608	3.16	1.684	0.166	+0.72
f	-2.19	2.576	3.23	1.754	0.159	+0.72
h	-2.19	2.585	3.23	1.753	0.149	+0.72
s	-2.27	1.166	...	...	...	+0.81
$\Theta = 0.33$ ML						
t	-1.93	2.577	2.97	1.494	0.398	+0.65
b	-1.98	2.594	3.17	1.694	0.189	+0.63
f	-1.98	2.726	3.24	1.764	0.001	+0.62
h	-1.98	2.723	3.24	1.764	0.005	+0.63
s	-2.06	1.630	...	...	...	+0.77

<sup>a</sup>Bader charge analysis on K adatoms.

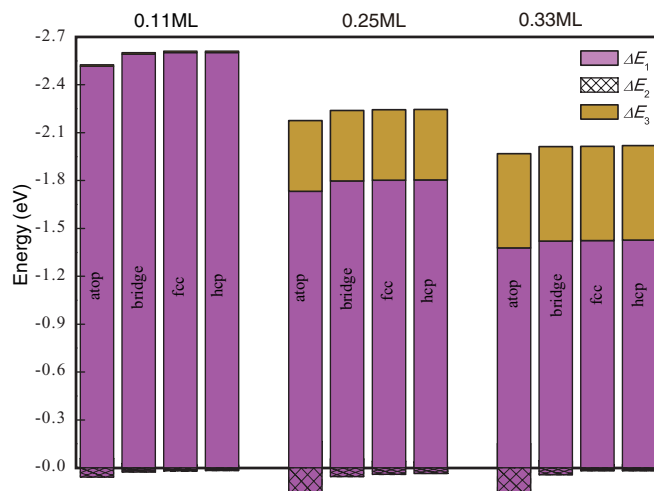


FIG. 2. The contributions from the bonding energy of K on the deformed Au(111) ( $\Delta E_1$ ), the energy cost of the surface deformation ( $\Delta E_2$ ), and the formation energy of one K atom from isolated gas phase to a K layer ( $\Delta E_3$ ) for K adsorption on Au(111) at  $\Theta_K = 0.11$  ML, 0.25 ML, and 0.33 ML. Of note, the mesh regions ( $\Delta E_2$ ) are located on the bottom of magenta ( $\Delta E_1$ ) bars to manifest the energy cost of surface deformation.

i.e., for one K atom ( $n = 1$ ), Eq. (1) is rewritten as

$$\begin{aligned}
 E_{\text{ads}} &= E_{\text{K/Au}} - E_{\text{Au(111)}} - E_{\text{K}} \\
 &= (E_{\text{K/Au}} - E_{\text{Au(111)-deformed}} - E_{\text{K-layer}}) \\
 &\quad + (E_{\text{Au(111)-deformed}} - E_{\text{Au(111)}}) + (E_{\text{K-layer}} - E_{\text{K}}) \\
 &= \Delta E_1 + \Delta E_2 + \Delta E_3,
 \end{aligned} \tag{7}$$

where  $E_{\text{Au(111)-deformed}}$  and  $E_{\text{K-layer}}$  represent the total energies of the Au(111) substrate with deformation including surface rumpling and lateral relaxation induced by K adsorption and the free-standing K layer. Consequently,  $\Delta E_1$  corresponds to the binding energy of K on the deformed Au(111),  $\Delta E_2$  is the energy cost of the surface deformation, and  $\Delta E_3$  is the formation energy of one K atom from isolated gas phase to a K layer. The results are summarized in Fig. 2.

It is clear that the first part, which is indicative of the direct K–Au chemical interactions, accounts for most of the K adsorption energy. This implies that the K–Au interaction plays the most important role in K–Au bonding process. Meanwhile, the contribution from the latter two becomes more and more evident as  $\Theta_K$  increased from 0.11 ML to 0.33 ML. Furthermore, the direct K–Au chemical interaction ( $\Delta E_1$ ) at atop is stronger than those at the other three sites at  $\Theta_K = 0.25$  and 0.33 ML. This is because K adsorption at the bridge and two hollow sites would suffer from more evident repulsion due to the bonding competition at higher coverage. However, the surface deformation for K at atop is the most drastic in all the cases, consuming the most energy. Therefore, the top-site adsorption is still the most unstable. These analysis may be also applied to elucidate the site preference of AM adsorption on metal surfaces to a certain degree.<sup>1</sup>

The bond length of K on Au(111) is similar to those of K on other fcc metal surfaces (Ag and Pd etc.):<sup>12,15</sup> it is the shortest for K on atop, longer at bridge, and the longest at the two hollow sites. Accordingly, the calculated effective K radii

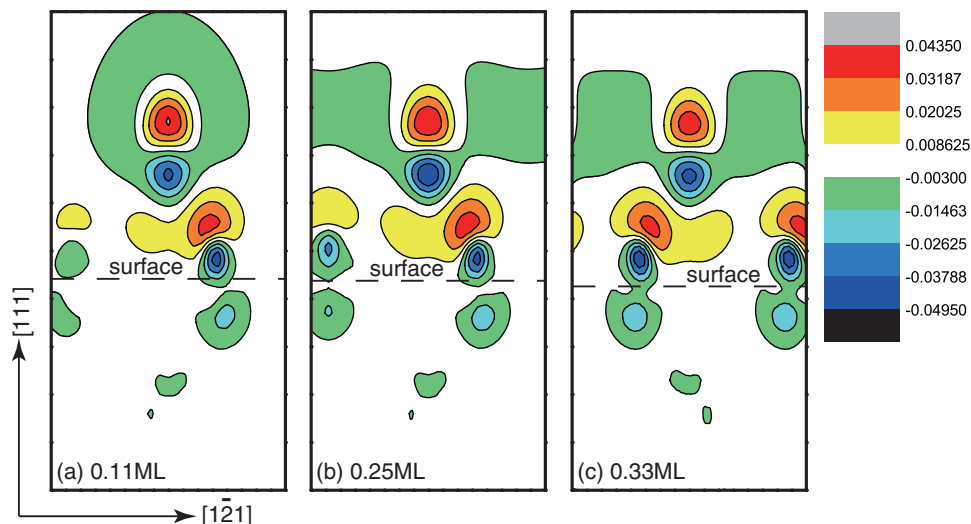


FIG. 3. Charge density difference contours of (a) 0.11 ML K, (b) 0.25 ML K, and (c) 0.33 ML K at hcp site. Contours with warm and cold colors correspond to charge accumulation and depletion, respectively.

( $R_{\text{eff}} = d_{\text{K-Au}} - 4.176/\sqrt{8}$ ) are the longest at the two hollow sites. The three K–Au bond lengths for K at hcp are 3.31 Å (0.11 ML), 3.23 Å (0.25 ML), and 3.24 Å (0.33 ML), respectively, and therefore the corresponding deduced effective K radii are 1.834, 1.754, and 1.764 Å. Additionally, the surface rumpling for K at atop site was found to be most obvious. The main effect of surface rumpling is to make the alkali adatoms closer to the surface, and thus coordinated with more substrate atoms. The calculated surface rumpling for K at hcp is 0.046, 0.159 Å in the  $(3 \times 3)$ -K and  $(2 \times 2)$ -K phases, respectively, while it is zero in  $(\sqrt{3} \times \sqrt{3})R30^\circ$ -K due to the equivalency of all the outermost layer Au atoms at the coverage. Nevertheless, to the best of our knowledge, there were no available experimental structural data in literature.

In order to further understand the K–Au interactions at the three studied  $\Theta_{\text{K}}$ , the projected density of states of K atom and the bonded Au atom for K at hcp were calculated (not shown here). Similar to other AM/TM cases, i.e., Na/Pd(111),<sup>44</sup> after K adsorption, part of its valence electrons is transferred to the substrate without much modification of the surface band features, suggesting that the donated electrons are rather delocalized. Meanwhile, the valence bands of K were found crossing the Fermi level, indicative of the metallic nature of K adlayer. To visualize the detailed charge redistribution upon K adsorption, charge density difference contours and planar averaged charge difference for K at hcp are plotted in Figs. 3 and 4, respectively. In the charge density difference, the  $(3 \times 3)$ -K system demonstrates some different features, namely, the charge depletion ( $4s$  electrons) mainly around the K center and extending to the vacuum region much farther, while in the latter two cases  $4s$  is depleted and delocalized almost in the K layer. In addition, some similar characters can be also found in the three cases. First, an evident charge accumulation can be observed in the interface region between K and Au. The  $p$ -like electrons of K are polarized towards the surface. From the planar averaged charge difference, it is evident that the charge redistribution mainly takes place in the first two Au layers and the K layer in all the cases:

charge accumulation between the first Au layer and K adlayer while depletion in the K layer further extending to the vacuum region, giving rise to an outward dipole. Furthermore, both the charge redistribution amount and the depletion range decrease with increasing K coverage, suggesting a depolarization of the K adatoms due to their increasing interactions. Bader charge analysis<sup>45</sup> indicates that the K adatoms are all partially positively charged, and the amount decreases as K coverage increases from 0.11 ML to 0.33 ML. Conclusively, these results revealed that the binding of K on Au(111) is an ionic bonding with some metallic characters at the three considered coverages.

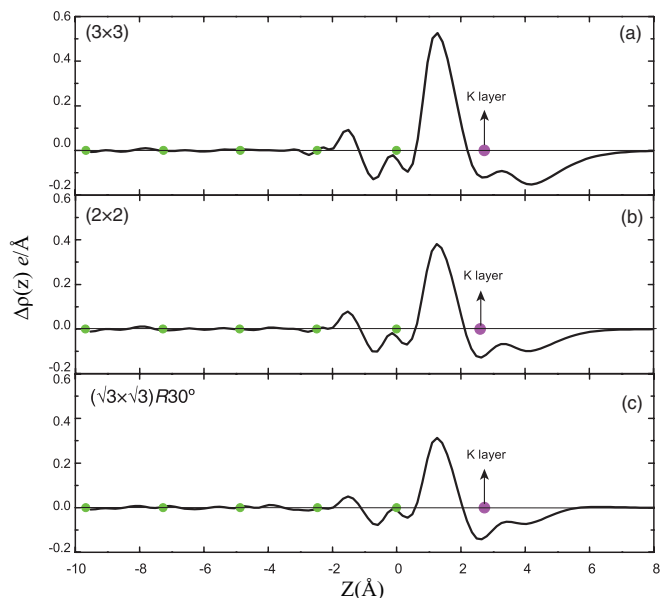


FIG. 4. Planar averaged charge changes of (a) 0.11 ML K, (b) 0.25 ML K, and (c) 0.33 ML K at hcp site. The average locations of each layer are indicated by the solid circles: smaller ones stand for the Au layers, while the bigger ones indicate the K layers. The height ( $Z$ ) of surface layer is set to zero.

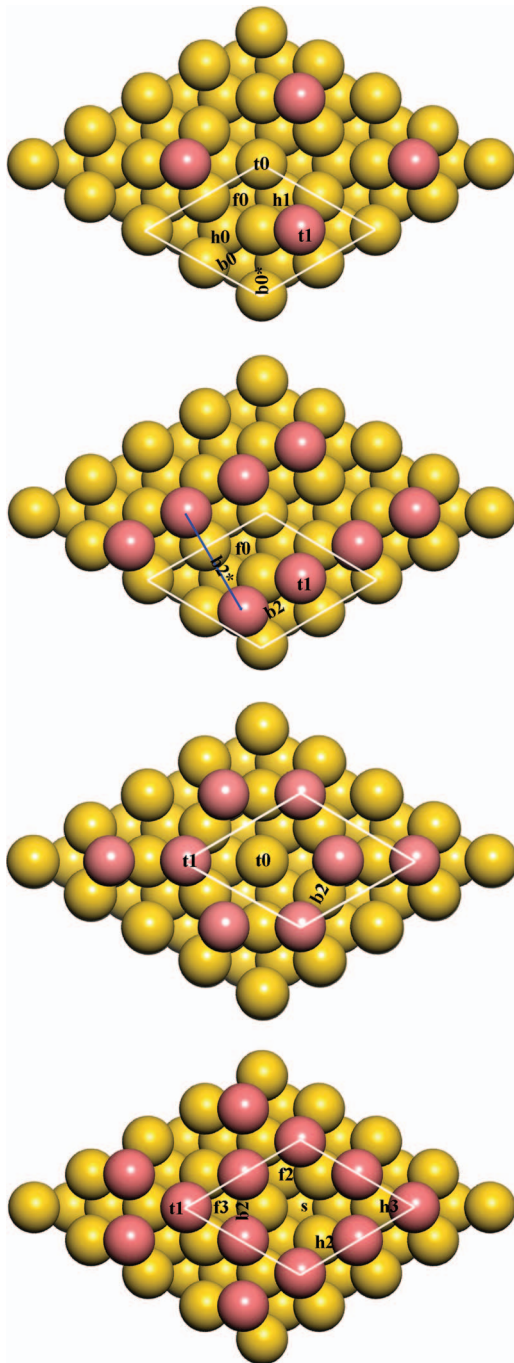


FIG. 5. Possible adsorption configurations for the K–Au intermixed structures. (a) One Au adatom at fcc; (b) two Au adatoms at fcc; (b<sup>\*</sup>) two Au adatoms with one at fcc and the other at hcp; (c) and three Au adatoms at fcc. The  $(2 \times 2)$  unit cell is shown by the white lines. The letters “t,” “b,” “f,” “h,” and “s” stand for the top, bridge, fcc, hcp, and substitutional sites. The numbers “0,” “1,” “2,” and “3” indicate number of Au adatoms the adsorbed K may bond to. The star “\*” is used to distinguish the same type sites with different distances to the adsorbed K atoms. In (b), b2<sup>\*</sup> is a long bridge site between two non-adjacent Au adatoms (blue line). The gold adatoms are marked by the red balls to guide the eye.

## B. Intermixed Au–K $(2 \times 2)$ phase

In this section, we performed DFT calculations to explore the possible structures for the intermixed  $(2 \times 2)$  K/Au(111) phase. We restricted the structural test in a  $(2 \times 2)$  unit cell with  $\Theta_K = 0.25$  ML and 0.5 ML on the substrates containing

TABLE II. Total energies,  $E_{\text{tot}}(n, m)$ , adsorption energies,  $E_{\text{ads}}$ , and the energy cost for creating  $m$  gold atoms,  $E_{\text{cost}}(m)$ , for K adsorption at 0.25, 0.5 ML on Au(111) with  $m$  gold adatoms ( $m = 0, 1, 2, 3$ ). The unit is electron volt (eV). At each  $\Theta_K$  and  $\Theta_{\text{Au}}$ , only the lowest energy results are listed. The adsorption sites for K are defined in Fig. 5.

		$n$ (ML) K							
		0.25 ML			0.5 ML				
m(ML)	Au	Site	$E_{\text{tot}}$	$E_{\text{ads}}$	$E_{\text{cost}}$	Site	$E_{\text{tot}}$	$E_{\text{ads}}$	$E_{\text{cost}}$
0.00		f	-2.19	-2.19	0	f + h	-2.95	-2.95	0
		h	-2.19	-2.19	0				
0.25 (f)		h0	-2.08	-2.73	0.65	t0 + h0	-3.66	-4.31	0.65
0.5 (f + f)		f0	-1.95	-2.71	0.76	f0 + f0	-2.89	-3.65	0.76
0.5 (f + h)		t0	-1.84	-2.98	1.14	b2 + t0	-3.08	-4.21	1.14
0.75 (f + f + f)		s	-2.25	-2.75	0.47	s + f3	-3.33	-3.80	0.47
						s + h3	-3.32	-3.80	0.47

0.00, 0.25, 0.5, and 0.75 ML of gold adatoms, as shown in Fig. 5. The results are summarized in Table II. The incorporation of  $m$  Au adatoms into a K layer can be observed only if

$$E_{\text{tot}}(n, 0) - E_{\text{tot}}(n, m) > 0, \quad (8)$$

where  $E_{\text{tot}}(n, 0)$  and  $E_{\text{tot}}(n, m)$  are the lowest adsorption energies for  $n$  K on the adatom-free and  $m$  Au adatoms covered surfaces, respectively. The gold adatoms were located at the fcc sites unless otherwise mentioned. The formation energies for creating 0.25, 0.5, 0.5(fcc + hcp), and 0.75 ML of gold adatoms are 0.65 eV, 0.76 eV, 1.14 eV, and 0.47 eV, respectively.

The binding of 0.25 ML K on Au surfaces with 0.25 and 0.5 ML gold adatoms is stronger than that on flat surface, but still not enough to compensate the cost to yield the Au adatoms. As for the surface with 0.75 ML Au atoms, namely, the surface with 0.25 ML Au vacancies, K adsorption at the substitutional site is a little more energetically favorable than the on-surface sites.

Then, we explored the possible configurations with 0.5 ML K adsorbed, as observed in the LEED pattern.<sup>24</sup> The first system we took into account was two K adsorptions on clean flat Au(111) surface (no Au adatoms). It was found that the configuration with one K at fcc and the other at hcp is the most energetically preferred, forming a honeycomb pattern on the surface. The average adsorption energy is  $-1.48$  eV/K. In the scenario of 0.5 ML K adsorption on the surface with 0.25 ML gold adatoms, it was found that the lowest energy configuration corresponds to one K at a surface top site (t0), and the other at h0, a honeycomb-like surface structure, as shown in the inset of Fig. 6. The average adsorption energy is  $-2.15$  eV, significantly lower than that of 0.5 ML K on the flat Au(111). Meanwhile, the binding is sufficiently enough to compensate the energy cost of Au adatoms formation.

Two types of substrates were considered to study the adsorption of 0.5 ML K on surfaces covered with 0.5 ML Au adatoms: both Au atoms at fcc sites [Fig. 5(b), denoted as 0.5(f + f) in Table II]; one Au at fcc and the other at hcp [Fig. 5(b<sup>\*</sup>), denoted as 0.5(f + h) in Table II]. The energy costs for creating two Au adatoms are 0.76 and 1.14 eV in the

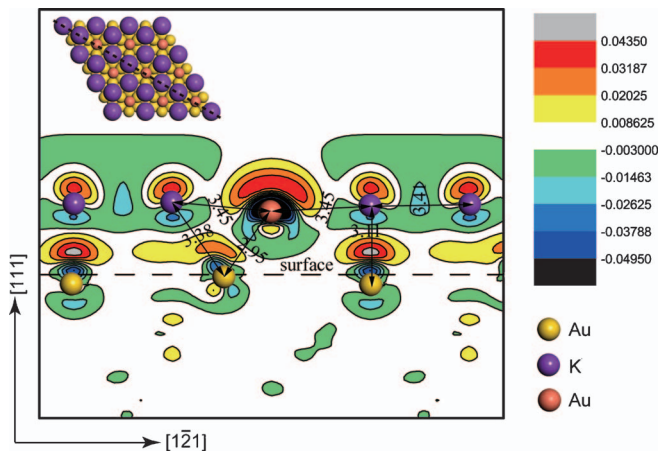


FIG. 6. Charge density difference contours for the most stable structure of K–Au intermixed layer. The cutting plane is shown in the upper left corner. Contours with warm and cold colors correspond to charge accumulation and depletion, respectively. The structural parameters (unit: Å) are shown correspondingly. The gold adatoms are marked by the red balls to guide eyes.

former and latter, respectively. However, 0.5 ML of K adsorption on the latter with one K at  $t_0$  and the other at  $b_2$  is more energetically stable than that on the former with the two K at two adjacent  $f_0$  sites,  $-2.11$  eV vs.  $-1.82$  eV per K. On the surface containing 0.75 ML of Au adatoms, we found that K also binds much more tightly to the surface compared to the Au adatom-free surface. Two energetically degenerate configurations are obtained to be the most energetically favorable: one K located at the substitutional site and the other K at either  $f_3$  or  $h_3$  [c.f. Fig. 5(c) and Table II]. The calculated average adsorption energy is  $-1.90$  eV per K in both configurations.

Generally, the adsorption of K on surfaces with defects is much stronger than that on clean flat surface, and the incorporation of gold atoms into adsorbate layer becomes feasible as the adsorbed K coverage increased to 0.5 ML (Table II), and an intermixed Au–K layer is formed. This is similar to the cases of electronegative atomic (e.g., Cl and O) adsorption on Au(111).<sup>38</sup> Furthermore, when taking into account the cost of forming Au adatoms, we found that the most energetically stable configuration is the 0.5 ML of K binding to the surface with 0.25 ML Au adatoms (c.f. the inset of Fig. 6). Therefore, we suggest that this model, which has a stoichiometry of  $K_2Au$ , may be the possible intermixed structure as observed in the LEED pattern.<sup>24</sup>

To get an insight of the stability of the  $K_2Au$  intermixed layer, the structural parameters and charge density difference contours were depicted in Fig. 6. Surprisingly, K–K distance of the nearest neighbor is 3.41 Å, much shorter than the value (4.52 Å) in bulk bcc K.<sup>46</sup> Meanwhile, this gives an average K radius of 1.71 Å, which is very close to its ionic radii (1.61 Å) in the potassium oxide ( $K_2O$ ).<sup>47</sup> Bader charge analysis indicates that both the K atoms are charged with  $+0.74e$ , while the charge of Au adatom is  $-0.93e$ . This deduces an ionic bond that may exist between K and Au adatoms. From the charge density difference plots, one can clearly observe that electrons deplete from K  $s$  orbital, while accumulate around the Au adatom as well as at the interface between the adlayer and the surface Au layer. Moreover, charge accumula-

tion around the Au adatom is much more notable, confirming the ionic bonding. It is expected that the ionic bonding minimizes the Coulomb repulsion between the two K ions, and thus lowers the total energy. In addition, the  $p$ -like electrons of K were found also polarized towards the surface as that in K on-surface adsorption. By the way, in this configuration, if the Au adatom and K at  $h_0$  change the adsorption site with each other, namely, Au adatom at a hcp while K at a fcc, the total energy is increased by only 15 meV, suggesting the possibility of the co-existence of the two configurations.

### C. Thermodynamic phase diagram of the K/Au(111) system at $\Theta_K = 0.11$ –0.5 ML

We now turn to investigate the temperature and pressure effects on the stability of the various K/Au structures. At each  $\Theta_K$ , the energetically preferred structures can be found in Tables I and II, namely, K at hcp or fcc for 0.11 ML K on clean flat Au(111), K at the substitutional site for 0.25 ML and 0.33 ML K on surfaces with Au vacancies, and the intermixed 0.5 ML K phase (c.f. the inset of Fig. 6) mentioned above. These structures are shown by the solid lines in Fig. 7(a), and denoted as 0.11 ML K, 0.25 ML K/0.25 ML Au vacancies, 0.33 ML K/0.33 ML Au vacancies, and 0.5 ML K/0.25 ML Au adatoms, respectively. The surface free energy as a function of  $\mu_K$  at  $\Theta_K = 0.11$ –0.5 ML is shown in Fig. 7(a). The K chemical potential is also correlated with the pressure at three selected temperatures, at which the LEED observations were made in Ref. 24. At a given temperature, higher  $\mu_K$  can be obtained by increasing the pressure of K gas.  $\mu_K$  should be less than the formation energy  $\mu_0$  of bulk K metal, which is calculated to be  $-1.12$  eV in bcc K bulk. For stable surface structures,  $\gamma$  should be less than zero. The K chemical potential in its bcc bulk reservoir ( $-1.12$  eV) is indicated by the vertical dashed line, while the clean surface ( $\gamma = 0$ ) is marked by the horizontal dashed line. It is clear that the coverage of K should be lower than 0.11 ML when  $\mu_K < -2.71$  eV, since the clean surface becomes more stable. For a slightly higher  $\mu_K$  (from  $-2.71$  eV to  $-2.14$  eV), K on-surface adsorption in the three-fold hollow sites (fcc or hcp) is the most stable. For  $\mu_K$  in the ranges of  $-2.14$  eV to  $-1.61$  eV and  $-1.61$  eV to  $-1.51$  eV, the substitutional adsorption at  $\Theta_K = 0.25$  and 0.33 ML becomes more stable, respectively. One may note that the substitutional adsorption is just  $\sim 3$  meV/Å<sup>2</sup> lower than the respective on-surface adsorption at 0.25 ML and 0.33 ML. When  $\mu_K > -1.51$  eV, the most stable surface structure changes to the  $(2 \times 2)$ –0.5 ML K intermixed layer. The transition around  $\mu_K = -1.51$  eV agrees well with the experiment observations showing the phase transition from  $(\sqrt{3} \times \sqrt{3})R30^\circ$  ( $\Theta_K = 0.33$  ML) to  $(2 \times 2)$  with  $\Theta_K = 0.5$  ML.

Figure 7(b) shows the two-dimensional ( $T, p$ ) phase diagram, in which only the lowest energy structures mentioned in Fig. 7(a) are presented. Generally, structures with higher  $\Theta_K$  can be observed by lowering the temperature or increasing the pressure of K. It is clear that the  $(3 \times 3)$ –0.11 ML on-surface adsorption has a very low thermal stability at temperatures between 300 and 400 K, since the required pressure is less than  $10^{-15}$  Torr, which is far below the operation pressure (i.e.,  $\sim 10^{-9}$  Torr). The  $(2 \times 2)$ –0.25 ML substitutional

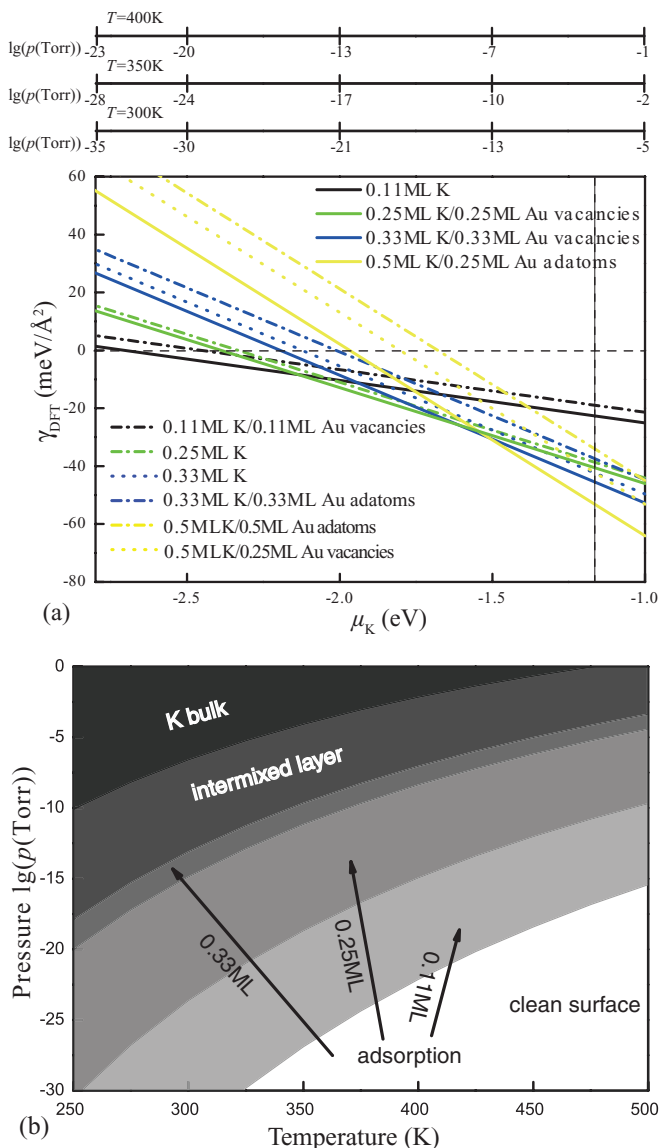


FIG. 7. (a) Surface free energies ( $\gamma_{\text{DFT}}$ ) as a function of the chemical potential of K ( $\mu_{\text{K}}$ ) at  $\Theta_{\text{K}} \leq 0.5$  ML on Au(111) with or without Au adatoms. The corresponding scales are shown for 3 selected temperatures. The energetically preferred adsorption configurations at each  $\Theta_{\text{K}}$  (cf. Tables I and II) are shown by the solid lines. (b) Calculated ( $T, p$ ) phase diagram for K/Au(111) system indicating the stable structures at  $\Theta_{\text{K}} = 0.11$ –0.5 ML.

adsorption might appear. However, the condition is still more or less strict ( $10^{-10}$  Torr at  $\sim 450$  K). Therefore, they can be safely excluded in the process of K adsorption on Au(111) under the operated condition in the experiment.<sup>24</sup> The  $(\sqrt{3} \times \sqrt{3})R30^\circ$ –0.33 ML phase is thermodynamically stable at about  $10^{-10}$  Torr and  $\sim 375$  K, and evolves to the  $(2 \times 2)$ –0.5 ML intermixed Au–K phase around  $10^{-9}$  Torr and  $\sim 375$  K. The reverse transition can be observed by raising the temperature. The phase diagram is in good agreement with the available LEED results:<sup>24</sup> clean surface  $\rightarrow (\sqrt{3} \times \sqrt{3})R30^\circ \rightarrow (2 \times 2)$  at room temperature with increasing K coverage, and  $(2 \times 2) \rightarrow (\sqrt{3} \times \sqrt{3})R30^\circ$  when the crystal temperature is raised to above  $\sim 450$  K. Furthermore, we note that the substitutional adsorption is a little more favorable than on-surface adsorption on the unreconstructed surface in the case of

$(\sqrt{3} \times \sqrt{3})R30^\circ$ –0.33 ML. This finding gives further support to the experimental result: K-induced Au atom release from the Chevron structure.

#### IV. CONCLUSIONS

Periodic density functional theory calculations combined with atomistic thermodynamics were employed to study the behaviors of K adsorption on Au(111) at coverages from 0.11 ML to 0.5 ML. Gold atoms can be readily pulled out of the surface upon K adsorption to form an intermixed Au–K layer when  $\Theta_{\text{K}} \geq 0.5$  ML. We suggested that the experimentally observed  $(2 \times 2)$  pattern may correspond to an intermixed layer with a stoichiometry of  $\text{K}_2\text{Au}$ , in which the first K adsorbs at an atop site, while the second K and the Au adatom occupy a fcc/hcp and a hcp/fcc, respectively. The calculated electronic structures demonstrated an ionic bonding with some metallic characters in the K–Au interaction. Further thermodynamic calculations showed an excellent agreement with the LEED observations, namely, the clean surface  $\rightarrow (\sqrt{3} \times \sqrt{3})R30^\circ \rightarrow (2 \times 2)$ , and reversely  $(2 \times 2) \rightarrow (\sqrt{3} \times \sqrt{3})R30^\circ$  by heating the sample.

#### ACKNOWLEDGMENTS

This work is supported by MOST under Project No. 2010CB631302 and the Fundamental Research Funds for the Central Universities, SCUT, under Project Nos. 2011ZG0017 and 2011ZM0090. The computing resources from the HPC Lab, Shenzhen Institute of Advanced Technology, Chinese Academy of Sciences (CAS), and ScGrid of the Supercomputing Center, Computer Network Information Center of CAS, are gratefully acknowledged.

- <sup>1</sup>R. D. Diehl and R. McGrath, *Surf. Sci. Rep.* **23**, 43 (1996).
- <sup>2</sup>R. D. Diehl and R. McGrath, *J. Phys.: Condens. Matter* **9**, 951 (1997).
- <sup>3</sup>A. Politano, A. R. Marino, and G. Chiarello, *J. Chem. Phys.* **132**, 044706 (2010).
- <sup>4</sup>A. H. Zhang, J. Zhu, and W. H. Duan, *Phys. Rev. B* **74**, 045425 (2006).
- <sup>5</sup>J. W. Gadzuk, *Phys. Rev. B* **79**, 073411 (2009).
- <sup>6</sup>Z. P. Liu and P. Hu, *J. Am. Chem. Soc.* **123**, 12596 (2001).
- <sup>7</sup>J. J. Mortensen, B. Hammer, and J. K. Nørskov, *Phys. Rev. Lett.* **80**, 4333 (1998).
- <sup>8</sup>J. J. Mortensen, B. Hammer, and J. K. Nørskov, *Surf. Sci.* **414**, 315 (1998).
- <sup>9</sup>S. J. Pratt, D. K. Escott, and D. A. King, *Phys. Rev. B* **68**, 235406 (2003).
- <sup>10</sup>C. Stampfl and M. Scheffler, *Surf. Sci.* **319**, L23 (1994).
- <sup>11</sup>G. G. Rusina, S. V. Eremeev, S. D. Borisova, I. Y. Sklyadneva, and E. V. Chulkov, *Phys. Rev. B* **71**, 245401 (2005).
- <sup>12</sup>K. Doll, *Phys. Rev. B* **66**, 155421 (2002).
- <sup>13</sup>J. M. Carlsson and B. Hellsing, *Phys. Rev. B* **61**, 13973 (2000).
- <sup>14</sup>G. Butti, S. Caravati, G. P. Brivio, M. I. Trioni, and H. Ishida, *Phys. Rev. B* **72**, 125402 (2005).
- <sup>15</sup>W. Z. Lai and D. Q. Xie, *J. Phys. Chem. B* **110**, 23904 (2006).
- <sup>16</sup>S. H. Ma, Z. Y. Jiao, T. X. Wang, and Z. X. Yang, *Eur. Phys. J. B* **75**, 469 (2010).
- <sup>17</sup>W. Z. Lai, W. Y. Huang, and D. Q. Xie, *Phys. Chem. Chem. Phys.* **10**, 1669 (2008).
- <sup>18</sup>S. More, W. Berndt, A. M. Bradshaw, and R. Stumpf, *Phys. Rev. B* **57**, 9246 (1998).
- <sup>19</sup>F. M. Pan, M. Caragiu, N. Ferralis, and R. D. Diehl, *Surf. Sci.* **600**, 537 (2006).
- <sup>20</sup>H. Brune, J. Winterlin, R. J. Behm, and G. Ertl, *Phys. Rev. B* **51**, 13592 (1995).
- <sup>21</sup>H. Tochihara and S. Mizuno, *Prog. Surf. Sci.* **58**, 1 (1998).

- <sup>22</sup>M. Haruta, T. Kobayashi, H. Sano, and N. Yamada, *Chem. Lett.* **16**, 405 (1987).
- <sup>23</sup>Y. Wang, N. S. Hush, and J. R. Reimers, *Phys. Rev. B* **75**, 233416 (2007).
- <sup>24</sup>J. V. Barth, R. Schuster, R. J. Behm, and G. Ertl, *Surf. Sci.* **348**, 280 (1996).
- <sup>25</sup>G. G. Rusina, S. D. Borisov, S. V. Eremeev, and E. V. Chulkov, *Russ. Phys. J.* **53**, 396 (2010).
- <sup>26</sup>B. Hammer and J. K. Nørskov, *Adv. Catal.* **45**, 71 (2000).
- <sup>27</sup>G. Kresse and J. Hafner, *Phys. Rev. B* **47**, 558 (1993).
- <sup>28</sup>G. Kresse and J. Hafner, *Phys. Rev. B* **48**, 13115 (1993).
- <sup>29</sup>G. Kresse and J. Furthmüller, *Comput. Mater. Sci.* **6**, 15 (1996).
- <sup>30</sup>G. Kresse and J. Furthmüller, *Phys. Rev. B* **54**, 11169 (1996).
- <sup>31</sup>P. E. Blöchl, *Phys. Rev. B* **50**, 17953 (1994).
- <sup>32</sup>G. Kresse and D. Joubert, *Phys. Rev. B* **59**, 1758 (1999).
- <sup>33</sup>J. P. Perdew and W. Yue, *Phys. Rev. B* **33**, 8800 (1986).
- <sup>34</sup>J. P. Perdew, J. A. Chevary, S. H. Vosko, K. A. Jackson, M. R. Pederson, D. J. Singh, and C. Fiolhais, *Phys. Rev. B* **46**, 6671 (1992).
- <sup>35</sup>M. Methfessel and A. T. Paxton, *Phys. Rev. B* **40**, 3616 (1989).
- <sup>36</sup>L. Y. Gan, Y. X. Zhang, and Y. J. Zhao, *J. Phys. Chem. C* **114**, 996 (2010).
- <sup>37</sup>W. W. Gao, T. A. Baker, L. Zhou, D. S. Pinnaduwa, E. Kaxiras, and C. M. Friend, *J. Am. Chem. Soc.* **130**, 3560 (2008).
- <sup>38</sup>T. A. Baker, C. M. Friend, and E. Kaxiras, *J. Chem. Phys.* **130**, 084701 (2009).
- <sup>39</sup>K. Reuter and M. Scheffler, *Phys. Rev. B* **65**, 035406 (2001).
- <sup>40</sup>H. Shi and C. Stampfl, *Phys. Rev. B* **76**, 075327 (2007).
- <sup>41</sup>H. Zhang, A. Soon, B. Delley, and C. Stampfl, *Phys. Rev. B* **78**, 045436 (2008).
- <sup>42</sup>X. Yang and J. Ni, *Phys. Rev. B* **74**, 195437 (2006).
- <sup>43</sup>H. J. Monkhorst and J. D. Pack, *Phys. Rev. B* **13**, 5188 (1976).
- <sup>44</sup>L.-Y. Gan, R.-Y. Tian, X.-B. Yang, and Y.-J. Zhao, *Chem. Phys. Lett.* **511**, 33 (2011).
- <sup>45</sup>R. Bader, *Atoms in Molecules: A Quantum Theory* (Oxford University Press, New York, 1990).
- <sup>46</sup>C. Kittel, *Introduction to Solid State Physics* (Wiley, New York, 1986).
- <sup>47</sup>P. Touzain, F. Brisse, and M. Caillet, *Can. J. Chem.* **48**, 3358 (1970).